PRINCIPLES OF POLYMER PROCESSING

Second Edition

ZEHEV TADMOR

The Wolfson Department of Chemical Engineering
Technion-Israel Institute of Technology
Haifa, Israel

COSTAS G. GOGOS

Otto H. York Department of Chemical Engineering
Polymer Processing Institute
New Jersey Institute of Technology
Newark, New Jersey

Library of Congress Cataloging-in-Publication Data:

Tadmor, Zehev, 1937 - Principles of polymer processing / Zehev Tadmor, Costas G. Gogos. – 2nd ed. p. cm.
Includes index.
ISBN 0-471-38770-3 (cloth)
1. Polymers. 2. Polymerization. I. Gogos, Costas G. II. Title.
TP1087.T32 2006
668.9–dc22

2006009306

Printed in the United States of America

10 9 8 7 6 5 4 3 2 1

14 Stretch Shaping

In this chapter we discuss three common and important stretch or extensional flow-based shaping operations: melt fiber spinning, tubular film blowing, and blow molding. These operations take place downstream from the die. Another stretch-flow–type shaping method is thermoforming, which involves deformation of previously shaped polymer sheets or films into a desired shape. Since the principles of thermoforming are very similar to those of parison inflation discussed later in this chapter, we do not dwell on this shaping method.

Fiber spinning is a uniaxial extensional deformation process, which is the principal method of manufacturing synthetic fibers for the textile industry. It also provides a good example of the enormous significance of ''structuring'' polymeric chains during shaping for imparting unique properties to a product. In fact, fiber spinning is the quintessential example of the goal of modern polymer processing as a multidisciplinary activity, better termed ''macromolecular engineering,'' whose objective, as discussed in Chapter 1, is: ''to bridge the gap between science and technology in material processing using modeling and computation of the full thermo mechanical history during formation to quantitatively predict properties'' (1).

Film blowing and blow molding are shaping operations that produce most plastics films, bags, and bottles, respectively. Both processes involve two-dimensional elongational deformation of the polymer melt. Thermoforming is a versatile, relatively inexpensive shaping method used extensively for packaging applications, which also involves two-dimensional extensional deformation. In all these processes, the purpose of a mathematical analysis is to describe the kinematics and dynamics of the process, to predict the nature and source of instabilities that are characteristic of these unconfined deformation processes, and, as just stated, hopefully predict a priori final properties based on the thermal and deformational history.

14.1 FIBER SPINNING

Until the 20th century mankind was limited to natural fibers such as wool, cotton, linen, and for the rich, silk. The first man-made fiber was artificial silk rayon (1910), which was based on cellulose. The big jump came with the invention of nylon by Wallace Carothers, with commercial production starting in 1939, followed in the 1950s by acrylics (which, when mixed with cotton, produced the ''wash-and wear'' textiles), polyesters, and many others.

Principles of Polymer Processing, Second Edition, by Zehev Tadmor and Costas G. Gogos.

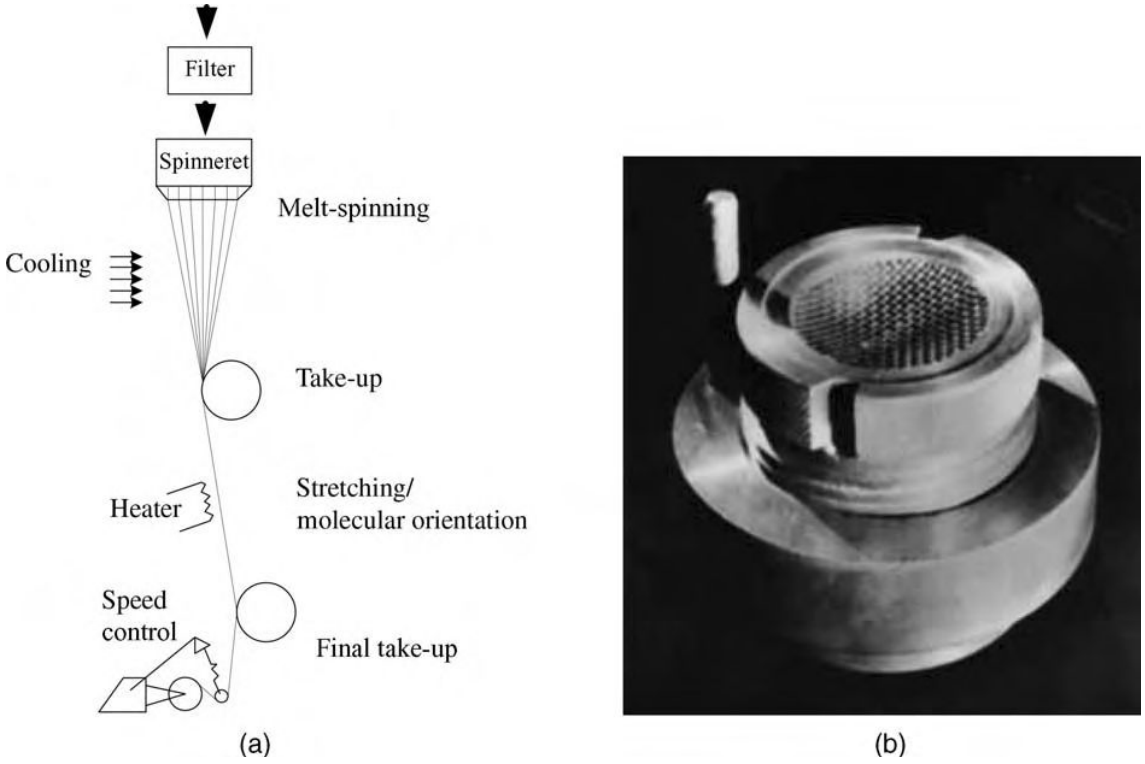

Fig. 14.1 (a) Schematic representation of the melt fiber spinning process. (b) Photograph of a spinneret. [Fiber-world Classroom Website.]

The melt spinning of fibers begins with the melting and pumping of solid pellets by a screw extruder (normally followed by a gear pump for accurate flow-rate control) into a die with multiple holes called a spinneret. The extruded strands are drawn and the solidified fibers are wound up and subsequently cold-drawn further, as shown schematically in Fig. 14.1(a). The design of a commercial spinneret is shown in Fig.14.1(b). In addition to melt spinning, there are two other spinning methods: wet spinning, in which the polymer is dissolved in a solvent and extruded through a spinneret immersed in a chemical solution, and dry spinning, which also extrudes a solution of the polymer the solvent of which evaporates upon exiting the spinneret. These are used for polymers that cannot be melt-spun. However, in this chapter we discuss only the ubiquitous and most commercially important melt spinning.

In analyzing the melt spinning process, we consider a single strand as it emerges from the spinneret and is drawn by the take-up roll, as shown in Fig. 14.2. There is no clear point of demarcation where post–die extrudate swelling ends and melt stretching begins. The two phenomena occur simultaneously, especially near the die exit, where the rapid rate of swelling ordinarily occurs. Experimental data from actual melt-spinning runs indicate that the melt strand cross-sectional area decreases hyperbolically from the spinneret exit to the take-up rolls (2). Figure 14.3 gives typical melt strand area and radius axial profiles. The melt drawdown region extends to about 200 cm from the spinneret exit. There is no specific indication of where the melt strand begins to solidify (‘‘frost line’’).

The final properties of the fiber, such as tenacity,[1] modulus, luster, and flex loss, are determined by the spinning process. This is because, as the molten filament moves from the spinneret exit to the take-up roll, it is simultaneously stretched and cooled, thus orienting the polymer chains (Fig. 14.4) and crystallizing the polymer; this is repeated with the subsequent drawing and orientation in the solid sate. Therefore, the

1. Tenacity equals the breaking strength (grams) divided by denier. Denier is the weight in grams of 9000 meters of filament.

spinning process is, in fact, not only a fiber forming step, but a ‘‘structuring’’ one as well. Early work on structuring during fiber spinning was done by Dees and Spruiell (3), who studied structure development with linear high density polyethylene fiber spinning and modeled it as shown in Fig. 14.5. They reported that the observed orientation function behavior during melt spinning can be explained with a morphological model, assuming that at low spin line stresses or take-up velocities, spherulitic structures are obtained. Increasing the take-up velocity results in row nucleated twisted lamellae, and at even higher speeds, in row nucleated untwisted lamellae.

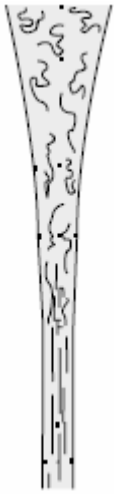

Fig. 14.4 Schematic view of orientation development along the spin line.

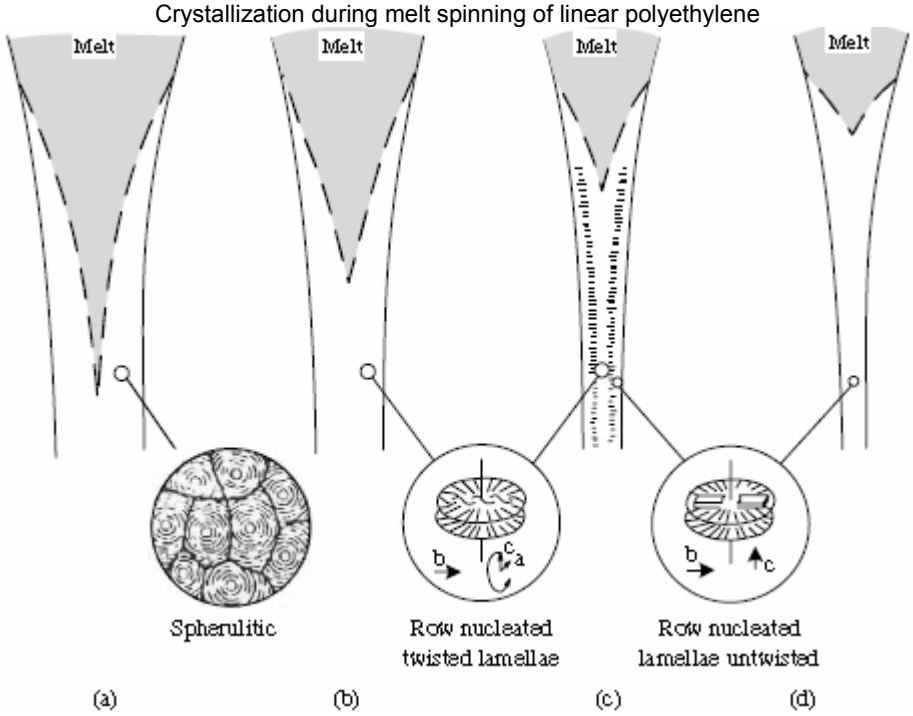

Fig. 14.5 Morphological model of structures developed in as-spun HDPE. Take-up velocities are (a) very low; (b) low; (c) medium; and (d) high. [Reprinted by permission from J. E. Spruiell and J. L. White, ‘‘Structure Development during Polymer Processing: Studies of the Melt Spinning of Polyethylene and Polypropylene Fibers,’’ Polym. Eng. Sci., 15, 660 (1975).]

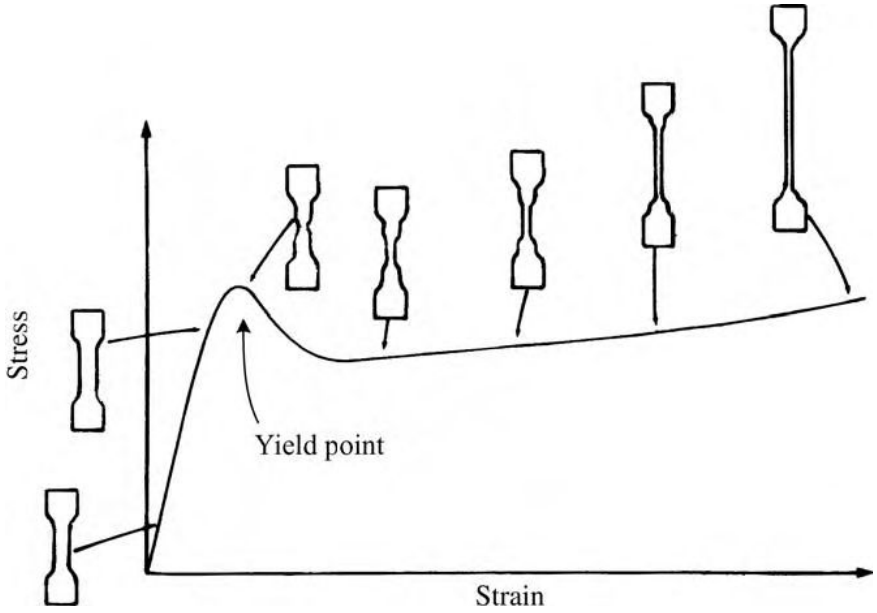

Fig. 14.6 Schematic stress–strain curves for a semicrystalline polymer. The shape of tensile specimens at several stages is indicated. [Reprinted by permission from J. M. Schultz, Polymer Materials Science, Prentice Hall, Englewood Cliffs, NJ, 1974.]

As noted in Fig.14.1(a), commercial fibers of semicrystalline polymers are always cold-drawn after spinning to achieve further structuring through further macromolecular orientation and crystalline morphological changes, many of which are retained because of the low temperature of the cold-drawing processes. A typical stress–strain curve for a polycrystalline polymer at a temperature Tg < T < Tm appears in Fig. 14.6.

The onset of yielding and necking of fibers, as well as films and tensile bar specimens, is the result of the ability of polycrystalline ‘‘composites’’ to accommodate stress-induced destruction of the crystalline units. In this process both the amorphous and the crystalline phases are involved. A ‘‘molecular’’ descriptive model of the morphological changes initiated with necking, and propagated by cold drawing, indicated in Fig. 14.7, consists of the following steps:

1. The lamellae slip rigidly past one another. Lamellae parallel to the direction of draw cannot slip; thus, spherulites become anisotropic. At this stage, at which necking begins, the strain is accommodated almost entirely by the interlamellar amorphous component.
2. Since the amorphous ‘‘ties’’ are almost completely extended, slip-tilting of the lamellae is induced.
3. Lamellar breakup occurs through chain pulling and unfolding; the chains pulled still connect the fragments of the lamellae.
4. The lamellar fragments slip further in the direction of draw and become aligned. They now form fibrils of alternating crystal blocks and stretched amorphous regions, which may also contain free chain ends, and some chain folds. Thus, the lamellae break into fragments that end up stacked in the axial direction. Tie molecules that connect these fragments in the draw direction provide the strength of the microfibrils in the fiber. Thus the goal in a fiber structuring operation is to employ the values of the parameters of spinning and drawing processes, which increase the fraction of tie molecules.

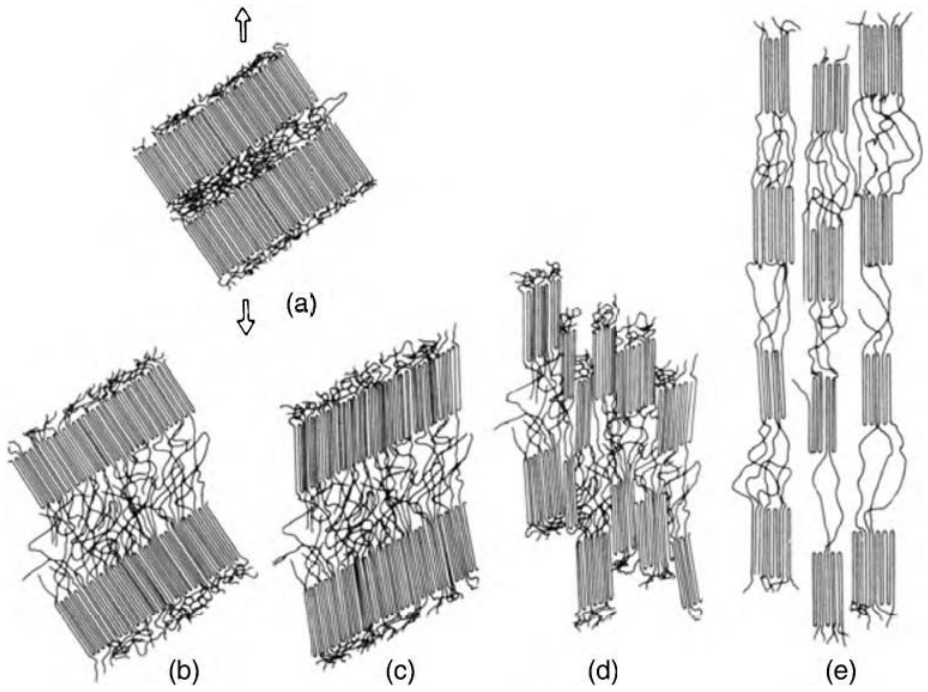

Fig. 14.7 Steps in the deformation of semicrystalline fiber, shown schematically. [Reprinted by permission from J. M. Schultz, Polymer Materials Science, Prentice Hall, Englewood Cliffs, NJ, 1974.]

It is evident from the preceding that the important cold drawing variables are not only the rate of extension, determining $t_{\exp} = 1/\dot{\varepsilon}$, and the temperature; determining the relaxation time, λ, but also the initial crystalline morphology, that is, the morphology obtained during the spinning process (see Fig. 14.5). Capaccio and Ward (4) demonstrated the important role played by the initial crystalline morphology in obtaining ultrahighly drawn and ultrahigh stiffness high density polyethylene (HDPE) fibers and films. A HDPE of $\overline{M}_n$ - 13,350 and $\overline{M}_w$ - 67,800, cooled from 160ºC and quenched at 110ºC, possessed an initial morphology such that, when drawn at 75ºC at 10 cm/min, it can be extended to a draw ratio of 30. The cold-drawn sample had a specific Young's modulus in tension E – 68 x 10^9 N/m², an order of magnitude higher than of conventionally drawn HDPE. For comparison, ''E'' glass fibers have a specific Young's modulus of 35 (N/m²) and Kevlar fibers, 92 (N/m²). It should be noted, however, that the theoretical estimates of Young's modulus for fully extended HDPE chains range from 240N/m² to 350 N/m² (4). Thus, further structuring improvements are possible, in principle.

The mathematical formulation of the fiber-spinning process is meant to simulate and predict the hydrodynamics of the process and the relationship between spinning conditions and fiber structure. It involves rapid extensional deformation, heat transfer to the surrounding quenching environment, air drag on the filament surface, crystallization under rapid axial-orientation, and nonisothermal conditions.

Example 14.1 A Semiempirical, Simplified, One-Dimensional, Nonisothermal Model [C. D. Han, Rheology in Polymer Processing, Academic Press, New York, 1976, Section 12.3.1.] Assuming steady state and further assuming that there is only one nonvanishing velocity component v(z), which is a function of only z, and that temperature varies only in the z direction, the equation of motion reduces to

$$v_z \frac{dv_z}{dz} - -v_z \frac{d}{dz}\left(\frac{\tau_{zz}}{\rho v_z}\right) - 2\left(\frac{\pi v_z}{\rho G}\right) F_D + g_z \qquad \text{(E14.1-1)}$$

where G - $\rho\pi R^2 v_z$ is the mass flow rate and F_D is the air drag force per unit area given by:

$$F_D = \left(\frac{0.843}{\pi R^2}\right)\left(\frac{\rho_a}{\rho}\right) G v_z \left[\frac{\pi \rho \mu_a}{\rho_a}\frac{(L-z)}{G}\right]^{0.915} \qquad \text{(E14.1-2)}$$

indicating that extension rate is controlled by tensile stresses, air drag on the fiber, and gravitational forces. Similarly, the equation of energy reduces to

$$\frac{dT}{dz} = -\frac{2}{C_v}\left(\frac{\pi}{\rho G v_z}\right)^{1/2}[h(T-T_a)+\sigma\varepsilon(T^4-T_a^4)] \qquad \text{(E14.1-3)}$$

In this equation, h is the heat transfer coefficient given by

$$\frac{hR}{k_a} = 0.21(1+K)\left(\frac{2R\rho_a v_z}{\mu_a}\right)^{0.334} \qquad \text{(E14.1-4)}$$

where K is an adjustable parameter and the subscript a refers to ambient air. According to Eq. E14.1-3 the temperature drop of the fiber depends on heat transfer to the ambient air and radiation losses. Han coupled these transport equations with an empirical ''Power Law in tension'' constitutive equation containing a temperature-dependent viscosity

$$\tau_{zz} = -3\alpha e^{\beta/T}\left[k_1 + k_2\left(\frac{dv_z}{dz}\right)^{n-1}\right]\frac{dv_z}{dz} \qquad \text{(E14.1-5)}$$

where

$$\alpha = \eta_0 e^{\Delta E/RT_0} = \eta_0 e^{\beta/T_0} \qquad \text{(E14.1-6)}$$

Many of the early models were one-dimensional, in which the field equations were averaged over the filament cross section. Kase and Matsuo (5,6) were the first to consider nonisothermal (in the stretching direction) fiber stretching. Matovich and Pearson (7) studied Newtonian, shear thinning and second order fluids. Denn at al. (8,9) modeled the process with upper-convected Maxwell constitutive equation. Papanastasiou et al. (10) studied isothermal viscoelastic spinning. Bell and Edie (11), using a finite element method (FEM), computed the two-dimensional temperature profile, assuming a one-dimensional velocity profile and measures of orientation, to obtain the internal stress distribution (12). The single component models were extended by Kulkarni and Beris (13) and Doufas et al. (14) to two component models, accounting for stress-induced crystallization.

A detailed two-dimensional numerical analysis of nonisothermal spinning of viscoelastic liquid with phase transition was carried out recently by Joo et al. (15). They used a mixed FEM developed for viscoelastic flows (16) with a nonisothermal version of the Giesekus constitutive equation (17), the Nakamura et al. (18) crystallization kinetics model, and the dependence of the crystallization rate on temperature and molecular orientation according to Ziabicki (19). They simulated amorphous polystyrene and fast-crystallizing nylon-6.6. The results indicate that although the kinematics in the thread line are approximately one-dimensional, as assumed by most researchers, the significant radial temperature nonuniformity leads to radially

nonuniform viscoelastic stresses, which result in radially nonuniform molecular orientation and strong radial variation of crystallinity.

The polystyrene simulation followed the experiments of Bell and Edie (12) with good agreement. Figure 14.8 shows the simulation results for fiber spinning nylon-6.6 with a draw ratio of 40. The figure demonstrates the wealth of information provided by the model. It shows the velocity, temperature, axial normal stress, and crystallinity fields along the threadline. We see the characteristic exponential-like drop in diameter with locally (radially) constant but accelerating velocity. However, results map out the temperature, stress, and crystallinity fields, which show marked variation radially and axially.

Recent advances in molecular dynamics simulations enabled Levine et al. (20) to take modeling one step further, to the molecular level. They succeeded in simulating from first principles the structure formation of 100 carbon atom polyethylene during uniaxial extension, under a variety of conditions. Figure 14.9 shows the dynamics of extensional deformation below the melting point, beautifully indicating the dynamic development of orientation and order.

Figure 14.10 shows the simulation results of nonisothermal crystallization, during simultaneous deformation and cooling through the melting point, as is the case in fiber spinning, indicating the formation of homogeneous, deformation-induced crystallization nuclei.

The foregoing analyses show, as pointed out earlier, that fiber spinning is perhaps the first process approaching the goal of modern polymer processing as macromolecular engineering. That is, developing a multiscale approach to simulate manufacturing processes using the governing continuum-level equations and operating conditions. Material-specific parameters for those equations are generated from molecular dynamics simulations, to ensure consistent, predictive ability. Crystal growth rates are generated using parameters derived entirely from first principles molecular modeling, over a large range of temperatures and molecular weight. This is shown schematically in Fig. 14.11.

So far, we assumed that the spinning process is stable. In practice, however, spinning instabilities may constrain spinning rates and even curb the possibility of spinning a fiber. Indeed, not all polymers can be melt-spun. Some polymers are easier to spin than others. The spinnability of a polymer is related to the stability of the process (21,22), particularly the ability of polymer melts to be drawn without breaking, due to either capillary failure resulting from surface tension–induced breakup into droplets, ‘‘necking’’ and ductile failure (23) characteristic to extension-thinning polymers, and/or cohesive fracture (24,25) exhibited by extension-thickening polymers.

A typical instability is *draw resonance*. Physically, the occurrence of draw resonance can be viewed as follows. In the region between the spinneret exit and the take-up rolls there can be a time variation of the total extrudate mass: although the rate of mass entering this region is constant, the rate it leaves is not controlled, since only the take-up speed is regulated, not the fiber diameter. Thus, if the strand thins out near the take-up rolls, the diameter of the strand above it will increase, creating (from the spinneret exit) a thick–thin strand. But the thick portion soon reaches the take-up rolls. Mass leaves the region at a high rate and the strands thin out upstream, creating a thin–thick strand. The process can repeat itself. This may explain the experimental reports that if solidification occurs before the take-up rolls, no resonance is observed (26), as well as the observation of increased resonance period with increased residence time in the spinline (21).

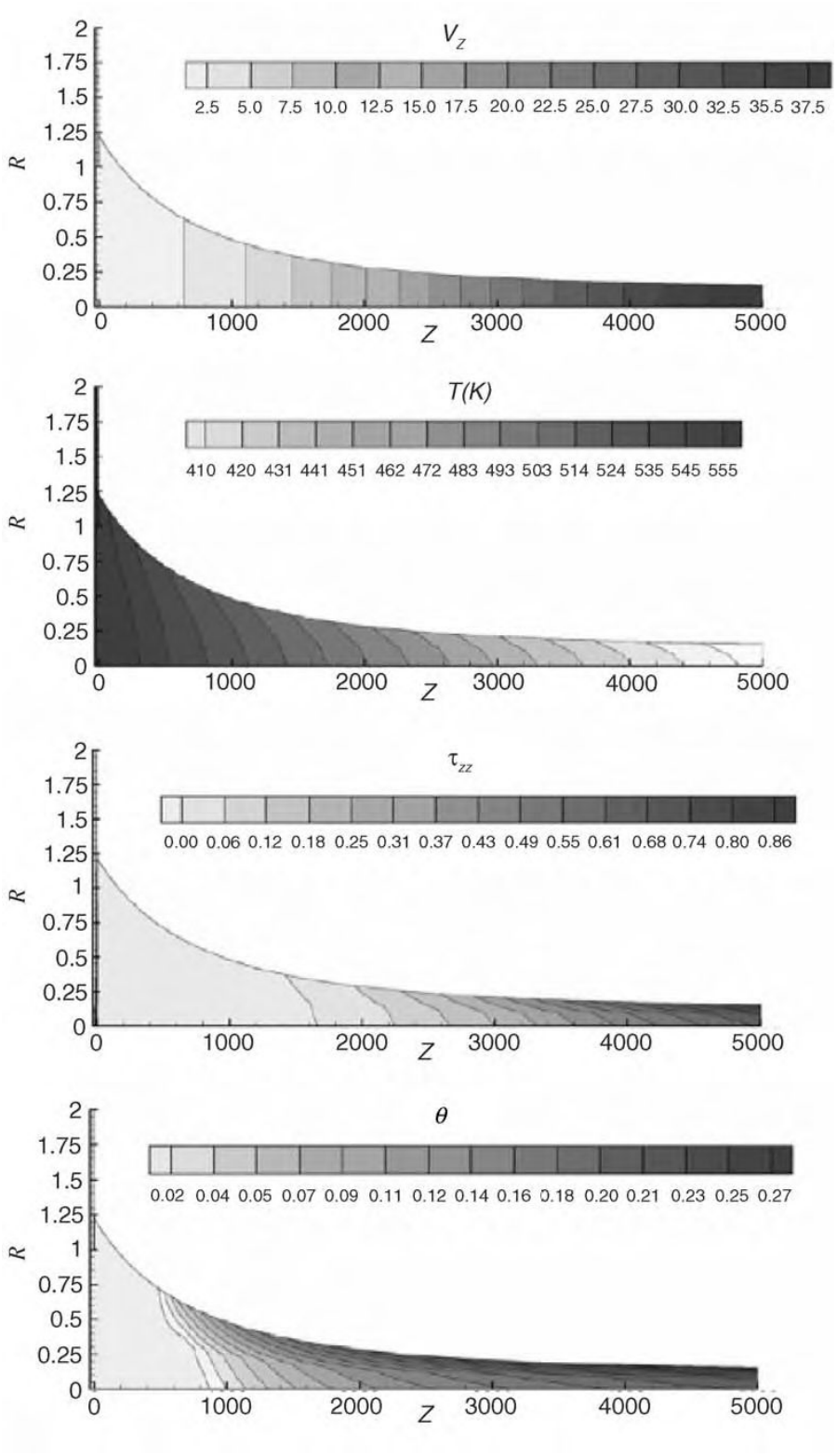

Fig. 14.8 Simulation results for velocity, temperature, axial normal stress, and crystallinity fields for low-speed spinning of nylon-6.6. [Reprinted with permission from Joo et al., ''Two-dimensional Numerical Analysis of Nonisothermal Melt Spinning with and without Phase Transition,'' *J. Non Newt. Fluid Mech*., 102, 37–70 (2002).]

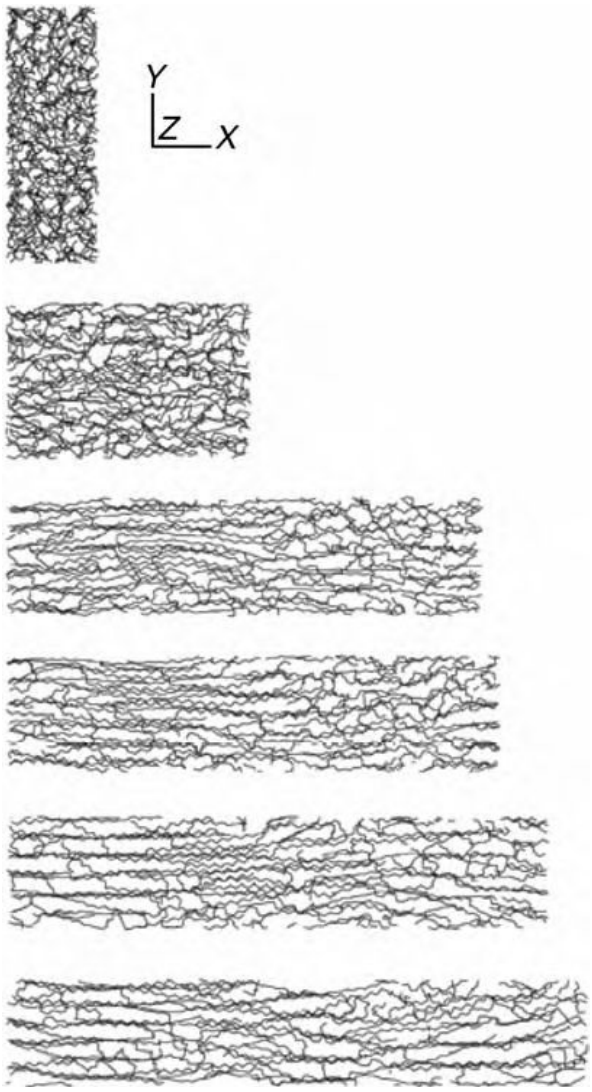

Fig. 14.9 Snapshots of a system of twenty 100 carbon atom long polyethylene chains deformed at 300 K. The initial slab at the top rapidly deforms with the applied stress in the x dimension of the slab, roughly doubling in the first 500 ps to λ - 2.64 (second image from the top); then the rate of deformation is slower and doubles again in 1500 ps to λ - 5.15 (third image from the top). Beyond this point the cell deforms even more slowly to reach a final deformation of λ - 6.28 (bottom image). In absolute values, the initial cell of dimensions 1.88 x 5.32 x 5.32 nm deforms to 11.8 x 2.23 x 1.96 nm. [Reprinted by permission from M. C. Levine, N. Waheed, and G. C. Rutledge, ‘‘Molecular Dynamics Simulation of Orientation and Crystallization of Polyethylene during Uniaxial Extension,’’ *Polymer*, 44, 1771–1779, (2003).]

Isothermal draw resonance is found to be independent of the flow rate. It occurs at a critical value of draw ratio (i.e., the ratio of the strand speed at the take-up rolls to that at the spinneret exit). For fluids that are almost Newtonian, such as polyethylene terephthalate (PET) and polysiloxane, the critical draw ratio is about 20. For polymer melts such as HDPE, polyethylene low density (LDPE), polystyrene (PS), and PP, which are all both shear thinning and viscoelastic, the critical draw ratio value can be as low as 3 (27). The maximum-to-minimum diameter ratio decreases with decreasing draw ratio and decreasing draw-down length.

The experimental and theoretical literature on instabilities in fiber spinning has been reviewed in detail by Jung and Hyun (28). The theoretical analysis began with the work of Pearson et al. (29–32), who examined the behavior of inelastic fluids under a variety of conditions using linear stability analysis for the governing equations. For Newtonian fluids, they found a critical draw ratio of 20.2. Shear thinning and shear thickening fluids exhibit critical draw ratios that are smaller or larger, respectively, than

20.2. At the same time, Denn et al. (8,33–36) systematically carried out both infinitesimal (linearized) and finite amplitude analyses of the isothermal draw resonance problem. They found that Newtonian fluids are stable to finite amplitude disturbances for draw ratios of less than 20.2. Linearized stability analysis revealed that for fluids that obey a White–Metzner-type constitutive equation, the critical draw ratio depends on the Power Law index n and the viscoelastic dimensionless number *N*

$$N = 3^{(1-s/2)}\left(\frac{m}{G}\right)^{s}\left(\frac{V_0}{L}\right) \qquad (14.1\text{-}1)$$

where $s = 1/n$, L is the spinline length, G is the tensile modulus, and V_0 is the spinneret velocity. The results appear in Fig. 14.12. Of interest is the ‘‘nose’’ region of the curves, which indicates that one could eliminate the draw resonance phenomenon by an increase in the draw ratio. Also of interest is the work of Han (37), who finds experimentally that as the temperature level is decreased in isothermal spinning, draw resonance occurs at lower draw ratios. This seems reasonable from the figure. In the ‘‘nose’’ region, decreasing the temperature increases *G* and decreases m, which in turn decreases *N*, bringing about lower draw ratio values.

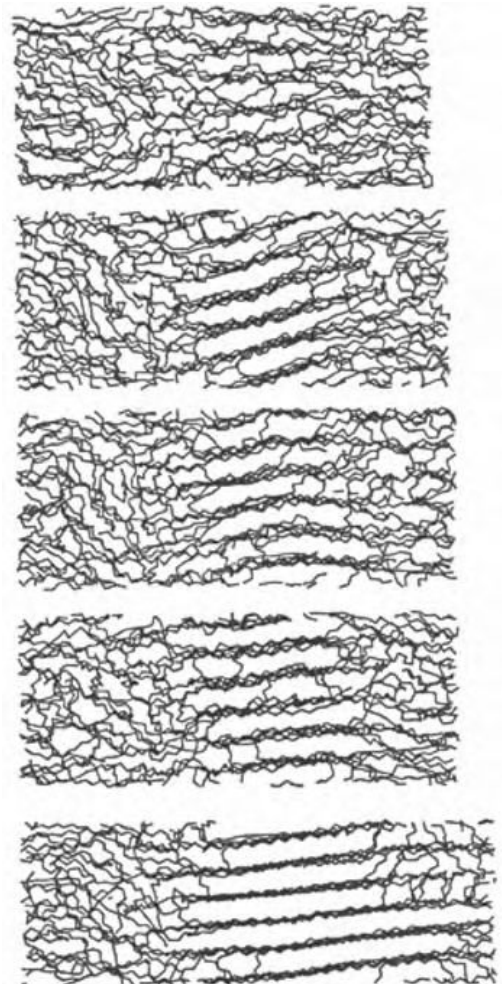

Fig. 14.10 Chain configurations from a nonisothermal deformation simulation. From top to bottom, the images were taken at 374, 368, 364, 360 K, and 290 K, corresponding to 7.6, 8.2, 8.6, 9.0, and 16.0 ns. [Reprinted by permission from M. C. Levine, N. Waheed, and G. C. Rutledge, ‘‘Molecular Dynamics Simulation of Orientation and Crystallization of Polyethylene during Uniaxial Extension,’’ *Polymer*, 44, 1771–1779, (2003).]

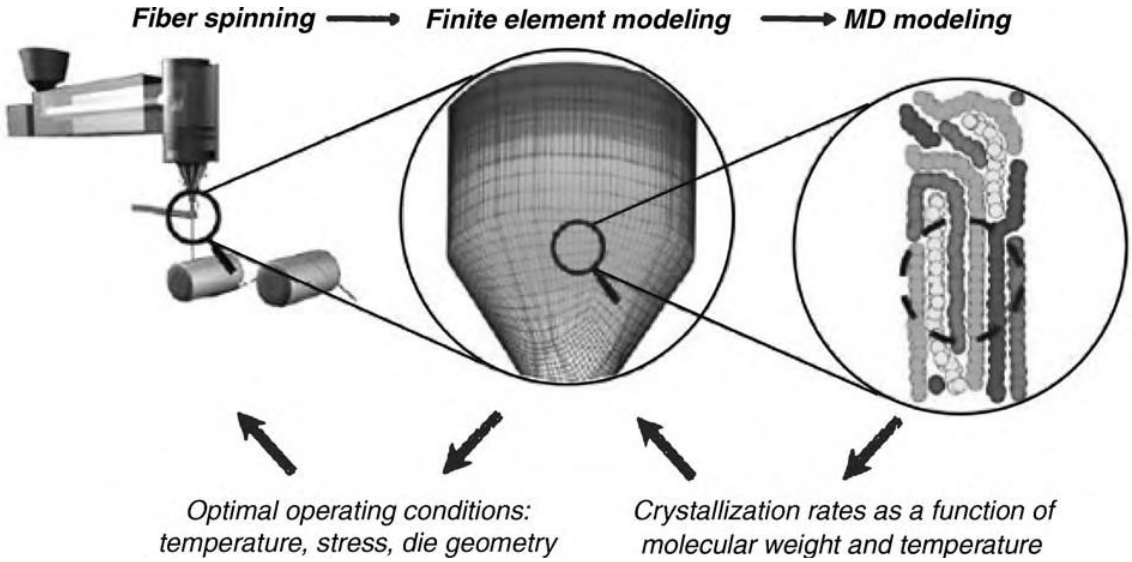

Fig. 14.11 Schematic representation of fiber spinning process simulation scheme showing the multiple scale simulation analysis down to the molecular level. This is the goal of the Clemson University–MIT NSF Engineering Research Center for Advanced Engineering Fibers and Films (CAEFF) collaboration. CAEFF researchers are addressing fiber and film forming and structuring by creating a multiscale model that can be used to predict optimal combinations of materials and manufacturing conditions, for these and other processes.

White et al. (38,39) presented experimental and theoretical (isothermal linear stability analysis) results that indicate the following: first, that polymer melts respond similarly to uniform elongational flow and to melt spinning; second, that polymers whose elongational viscosity $\eta^+(t,\dot{\varepsilon})$ increases with time or strain result in a stable spinline, do not exhibit draw resonance, and undergo cohesive failure at high draw ratios. A prime example of such behavior is LDPE. On the other hand, polymer melts with a decreasing $\eta^+(t,\dot{\varepsilon})$ exhibit draw resonance at low draw ratios and break in a ductile fashion (after ‘‘necking’’) at high draw ratios. Typical polymers in this category are HDPE and PP.

The preceding analyses were based on steady state solution of the governing equations, and examining the response of the system to applied sinusoidal perturbations. However, for the study of the dynamics of the instability, and for tracing the physical sources of instability, transient time-dependent solutions are needed. Hyun et al. (40,41) developed such solutions by tracing and analyzing kinematic traveling waves on the spinline from the spinneret to the take-up. Their simulation shows good agreement with the experiments (28).

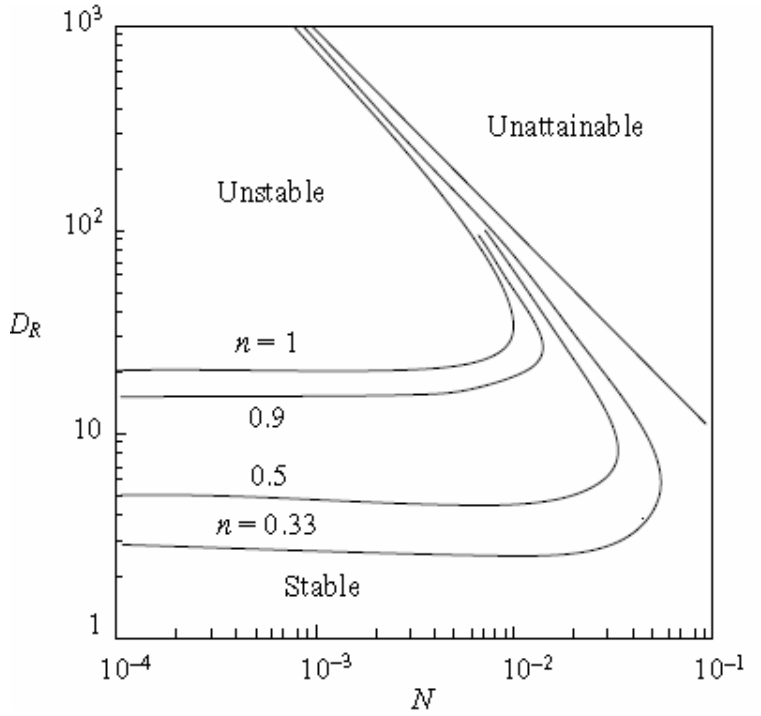

Fig. 14.12 Results of the linearized stability analysis for a White–Metzner-type fluid, indicating the dependence of the critical draw ratio on n and N. [Reprinted by permission from R. J. Fisher and M. M. Denn, ‘‘A Theory of Isothermal Melt Spinning and Draw Resonance,’’ AIChE J., 22, 236 (1976).]

14.2 FILM BLOWING

Most films and bags, in sizes varying from a sandwich bag to large films covering building sites, are made by the ingenious and deceptively simple process of film blowing. This process is shown schematically in Fig. 14.13(a), and a photograph of the process is shown in Fig. 14.13(b). A relatively small diameter tubular film is extruded upwards; upon exit it is blown up, with air introduced below the die, into a larger tubular film and then picked up by a pair of nip rolls that seal the bubble. An external stream of chilled air cools and solidifies the film at a certain upstream location called the freeze line, where T_f - T_m. In this process the film is stretched biaxially, thereby improving its mechanical properties. The blow up ratio, R_f / R_0, determined by the pressure level within the bubble, sets the (tangential) circumferential stretching, and the speed of take-up by the nip rolls sets the axial stretching.

The film thickness produced by film blowing ranges from 10 μm to 100 μm and the rates of production are very high. The most common plastic films produced by this method are branched LDPE, linear low density polyethylene (LLDPE), and linear HDPE films. By using more than one extruder, multilayer films can also be manufactured. To appreciate the elegant engineering simplicity of this process, we have to compare it to the more complicated and expensive die forming flat film process, where the melt is extruded through a slit die onto chilled take-up rolls. The latter process, while more expensive, has the advantage of producing optically clear films, because of the profuse nucleation induced by the quenching abilities of the chilled rolls. Yet, as the mathematical analysis discussed below demonstrates, the film blowing process is not simple at all, particularly when we consider the multiplicity of steady states and bubble instabilities that may arise which, in addition to cooling rates, place upper limits on production rates.

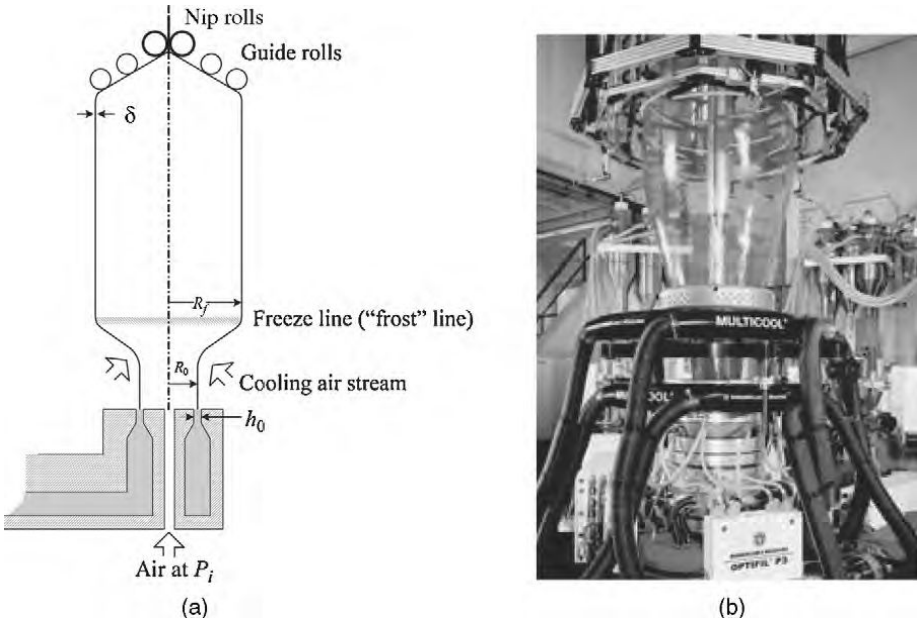

Fig. 14.13 (a) Schematic representation of the tubular blown film forming operation. (b) Photograph of a coextruded blown film die followed by blown film with external and internal cooling. [Courtesy of Windmoeller & Hoelscher (Lincoln RI).]

The first milestone in modeling the process is credited to Pearson and Petrie (42–44), who laid the mathematical foundation of the thin-film, steady-state, isothermal Newtonian analysis presented below. Petrie (45) simulated the process using either a Newtonian fluid model or an elastic solid model; in the Newtonian case, he inserted the temperature profile obtained experimentally by Ast (46), who was the first to deal with nonisothermal effects solve the energy equation to account for the temperature-

dependent viscosity. Petrie (47) and Pearson (48) provide reviews of these early stages of mathematical foundation for the analysis of film blowing.

Han and Park (49–51) used a coupled force and thermal energy balances to take care of the nonisothermal nature of the process and accounted for the non-Newtonian nature of the viscosity. Gupta (52) presented experimental results that were used by several investigators. Kanai and White (53, 54) carried out detailed experimentation as well as theoretical analysis of both the kinematics and the dynamics of the process and the effect of the cooling rate on crystallization. Heat transfer and bubble cooling were studied by Sidiropoulos and Vlachopoulos (55–58), who used numerical simulation to study air flow around the bubble, investigated the effect of internal bubble cooling, and studied the temperature gradient in the blown film. Finally, Campbell et al. (59) carried out a full aerodynamic analysis of the cooling air around the bubble.

The early attempts to account for the viscoelastic nature of the fluid encountered mathematical difficulties in the numerical solutions. Yet later, Luo and Tanner (60) expanded the Petrie model to viscoelastic nonisothermal flow using the convected Maxwell and Leonov (61) models, and compared results to experiments done by Gupta (52). Cain and Denn (62) carried out a detailed analysis of both Newtonian and viscoelastic fluids. For the latter, they used the upper convected Maxwell model and the Marruci (63) model. They found that multiple solutions of the governing equations are possible even for the Newtonian fluid, with the existence of more than one steady state bubble profile for a given set of operating conditions. Furthermore, they found several types of instabilities. A recent, detailed review of film blowing instabilities is given by Jung and Hyun (28).

Following the principles of the Petrie model, and recalling that the film thickness δ is much smaller than the radius $\delta / R << 1$, we invoke the ‘‘thin-film approximation,’’ which implies that field equations are averaged over the thickness and that there are no shear stresses and moments in the film. The film is regarded, in fact, as a thin shell in tension, which is supported by the longitudinal force F_z in the bubble and by the pressure difference between the inner and outer surfaces, ΔP. We further assume steady state, a clearly defined sharp freeze line above which no more deformation takes place and an axisymmetric bubble. Bubble properties can therefore be expressed in terms of a single independent spatial variable, the (upward) axial position from the die exit,[2] z. The object of the analysis is to predict the dependent variables, including the bubble radius, film thickness, film temperature (in the nonisothermal case), and local values of stresses as a function of the axial distance, z.

We first derive the kinematics of the deformation. The flow situation is shown in Fig. 14.14. Coordinate z is the vertical distance in the center of the axisymmetric bubble with the film emerging from the die at $z - 0$. The radius of the bubble R and its thickness δ are a function of z. We chose a coordinate system ξ_i embedded in the inner surface of the bubble. We discussed extensional flows in Section 3.1 where we defined the velocity field of extensional flows as

$$v_i - a_i \xi_i \qquad (14.2\text{-}1)$$

2. To be exact, the origin of variable z is located not at the die exit, but just past the die-exit swell region (21).

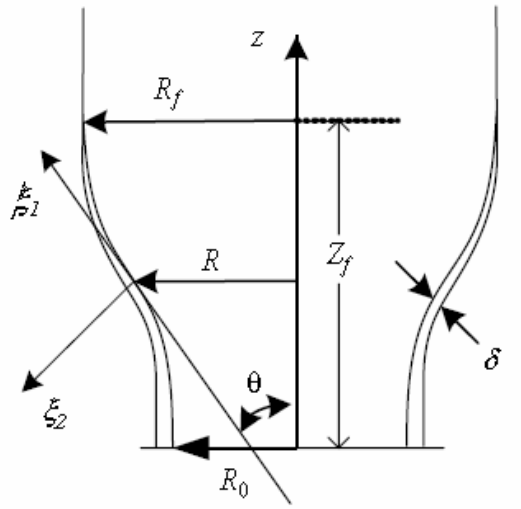

Fig. 14.14 The melt exits the die at *z - 0*; the radius of the bubble *R* and the thickness δ are a function of *z*. The coordinate system ξ_1 is embedded into the inner surface of the bubble.

In this case, as pointed out earlier, the extension is planar, but unequal in directions ξ_1 and ξ_3. In order to derive the rate of deformation tensor components, we need to define the flow field in terms of the dependent variables δ and *R*. We note that in direction *"2"* at $\xi_2 - \delta$, we can write

$$v_2 - a_2\delta - \frac{d\delta}{dt} \tag{14.2-2}$$

Writing a_2 in terms of δ, from the kinematics of extensional flow, we have

$$\dot{\gamma}_{22} - 2a_2 - \frac{2}{\delta}\frac{d\delta}{dt} \tag{14.2-3}$$

We can rewrite Eq. 14.2-3 as follows

$$\dot{\gamma}_{22} - 2a_2 - \frac{2}{\delta}\frac{d\delta}{d\xi_1}\frac{d\xi_1}{dt} \tag{14.2-4}$$

where

$$\frac{d\xi_1}{dt} - v_1 \tag{14.2-5}$$

And from geometrical considerations, we find that

$$\frac{d\delta}{d\xi_1} - \frac{d\delta}{dz}\frac{dz}{d\xi_1} - \cos\theta\frac{d\delta}{dz} \tag{14.2-6}$$

Substituting Eqs, 14.2-6 and 14.2-5 into Eq. 14.2-4, we get

$$\dot{\gamma}_{22} - \frac{2}{\delta}v_1\cos\theta\frac{d\delta}{dz} \tag{14.2-7}$$

The volumetric flow rate Q is given by

$$Q - 2\pi R\delta v_1 \tag{14.2-8}$$

Substituting it into Eq. 14.2-7, we obtain

$$\dot{\gamma}_{22} - \left(\frac{Q\cos\theta}{\pi R\delta}\right)\frac{1}{\delta}\frac{d\delta}{dz} \tag{14.2-9}$$

The film circumference at any given z where the bubble radius is R, is $l - 2\pi R$, and the velocity v_3 is given by

REFERENCES

1. J. F. Agassant, P. Coates, M. Denn, D. Edie, C. G. Gogos, K. S. Hyun, M. Kamal, H. Meijer,W. Michaeli, D. H. Sebastian, Z. Tadmor, J. Vlachopoulos, J. L. White, andM. Xanthos, (Organizing Committee), ''Touchstones of Modern Polymer Processing,'' Workshop Held at the Polymer Processing Institute at New Jersey Institute of Technology, Newark NJ, May 10–12, 2002. The quote is due to Han Meijer.
2. H. F. Mark, in Rheology, Vol. 4, F. R. Eirich, Ed., Academic Press, New York, 1969, Chapter7.
3. J. R. Dees and J. E. Spruiell, ''Structure Development During Melt Spinning of Linear Polyethylene Fiber,'' J. Appl. Polym. Sci. 18, 1053 (1974).
4. G. Capaccio and I. M. Ward, ''Ultra-high Modulus Linear Polyethylene through Controlled Modulus Weight and Drawing,'' Polym. Eng. Sci., 15, 219–224 (1975).
5. S. Kase and T. Matsuo, ''Studies on Melt Spinning, I. Fundamental Equations on the Dynamics of Melt Spinning,'' J. Polym. Sci., Part A, 3, 2541 (1965).
6. S. Kase and T. Matsuo, ''Studies on Melt Spinning, Part II. Steady State and Transient Solutions of Fundamental Equations Compared with Experimental Results, Fundamental Equations on the Dynamics of Melt Spinning,'' J. Appl. Poly. Sci., 11, 251–287 (1967).
7. M. A. Matovich and J. R. A. Pearson, ''Spinning a Molten Threadline,'' Ind. Eng. Fundam., 8, 512 (1969).
8. M. M. Denn, C. J. S. Petrie, and P. Avenas, ''Mechanics of Steady Spinning of Viscoelastic Liquids,'' AIChE J., 21, 791(1975).
9. R. J. Fisher and M. M. Denn, ''ATheory of Isothermal Melt Spinning and Draw Resonance,'' AIChE J., 22, 236–246 (1976).
10. T. C. Papanastasiou, C. W. Macosko, L. E. Scriven, and Z. Chen, ''Fiber Spinning of Viscoelastic Liquid,'' AIChE J., 33, 834–842 (1987).
11. P. W. Bell and D. D. Edie, ''Calculated Internal Stress Distribution in Melt-spun Fibers,'' J. Appl. Polym. Sci., 33, 1073–1088 (1987).
12. P.W. Bell and D. D. Edie, ''Measured Orientation and Internal Stress Distribution in Melt-spun Fibers,'' J. Appl. Polym. Sci., 33, 1089–1102 (1987).
13. J. A. Kulkarni and A. N. Beris, ''Lattice-based Simulation of Chain Conformation in Semicrystalline Polymers with Application to Flow Induced Crystallization,'' J. Non-Newt. Fluid Mech., 82, 331–336 (1999).
14. A. K. Doufas, A. J. McHugh, and C. Miller, ''Simulation of Melt Spinning Including Flowinduced Crystallization. Part I. Model Development and Predictions,'' J. Non-Newt. Fluid Mech., 92, 27–66 (2000).
15. Y. L. Joo, M. D. Smith, R. C. Armstrong, R. A. Brown, and R. A. Ross, ''Two-dimensional Numerical Analysis of Non-isothermal Melt Spinning with and without Phase Transition,'' J. Non-Newt. Fluid Mech., 102, 37–70 (2002).
16. R. Guennete and M. Fortin, ''A New Mixed Finite Element Method for Computing Viscoelastic Flows,'' J. Non-Newt. Fluid Mech., 77, 153–190 (1998).
17. H. Giesekus, ''A Simple Constitutive Equation for Polymer Fluids Based on the Concept of Deformation-dependent Tensorial Mobility,'' J. Non-Newt. Fluid Mech., 11, 60–109 (1982).
18. K. Nakamura, K. Katayama, and T. Amano, ''Some Aspects of Non-isothermal Crystallization of Polymers. Part II. Consideration of Isokinetic Conditions,'' J. Appl. Polym. Sci., 17, 1031–1041 (1982).
19. A. Ziabicki, Fundamentals of Fiber Formation, Wiley, New York, 1976.
20. M. C. Levine, N. Waheed, and G. C. Rutledge, ''Molecular Dynamics Simulation of Orientation and Crystallization of Polyethylene during Uniaxial Extension,'' Polymer, 44, 1771–1779 (2003).
21. Y. Ide and J. L. White, ''The Spinnability of Polymer Filaments,'' J. Appl. Polym. Sci., 20, 2511–2531 (1976).
22. C. J. S Petrie and M. M. Denn, ''Instabilities in Polymer Processing,'' AIChE J., 22, 209 (1976).
23. Y. Ide and J. L. White, ''Investigation of Failure during Elongational Flow of Polymer Melts,'' J. Non Newt. Fluid Mech., 2, 281–298 (1977).
24. J. L. White and Y. Ide, ''Instabilities and Failure in Elongational Flow of Melts in Isothermal Spinning of Fibers,'' J. Appl. Polym. Sci., 22, 3057–3074 (1978).
25. S. Lee, B. M. Kim, and J. C. Hyun, ''Dichotomous behavior of Polymer Melts in Isothermal Mel Spinning,'' Korean J. Chem. Eng., 12, 345–351 (1995).
26. S. Kase, ''Studies in Melt Spinning, IV. On the Stability of Melt Spinning,'' J. Appl. Polym. Sci., 18, 3279 (1974).
27. G. F Cruz-Saenz, G. J. Donnelly, and C. B. Weinberger, ''Onset of Draw Resonance during Isothermal Melt Spinning,'' AIChE J., 22, 441 (1976).
28. H. W. Jung and J. C. Hyun, ''Fiber Spinning and Film Blowing Instabilities,'' in Polymer Processing Instabilities – Control and Understanding, S. G. Hatzikiriakos and K. B. Migler,

Eds., Marcel Dekker, New York, 2004, Chapter 11.
29. J. R. A. Pearson and Y. T. Shaw, ‘‘Stability Analysis of the Fiber Spinning Process,’’ Trans. Soc. Rheol., 16, 519–533 (1972).
30. Y. T. Shaw and J. R. A. Pearson, ‘‘On the Stability of Non-isothermal Fiber Spinning – General Case,’’ Ind. Eng. Chem. Fundam., 11, 150–153 (1972).
31. J. R. A. Pearson and Y. T. Shaw, ‘‘On the Stability of Isothermal and Non-isothermal Fiber Spinning of Power Law Fluids, ‘‘ Ind. Eng. Chem. Fundam., 13, 134–138 (1974).
32. J. R. A. Pearson, Y. T. Shaw, and R. D. Mhaskar, ‘‘On the Stability of Fiber Spinning of Freezing Fluids, ‘‘ Ind. Eng. Chem. Fundam., 15, 31–37 (1976).
33. R. J. Fisher and M. M. Denn, ‘‘Finite-amplitude Stability and Draw Resonance in Isothermal Spinning,’’ Chem. Eng. Sci., 30, 1129–1134 (1975).
34. R. J. Fisher and M. M. Denn, ‘‘Mechanics of Nonisothermal Polymer Melt Spinning,’’ AIChE J., 23, 23–28 (1977).
35. J. C. Chang and M. M. Denn, ‘‘Sensitivity of the Stability of Isothermal Melt Spinning to Rheological Constitutive Assumptions,’’ in Rheology: Applications, Vol. 3., G. Astarita, G. Marrucci, and L. Nicolais, Eds., Plenum Publishing, New York 1980, pp.9–13.
36. J. C. Chang, M. M. Denn, and F. T. Geyling, ‘‘Effect of Inertia, Surface Tension and Gravity on the Stability of Isothermal Drawing of Newtonian Fluids,’’ Ind. Eng. Chem. Fundam., 20, 147–149 (1981).
37. C. D. Han, Rheology in Polymer Processing, Academic Press, New York, 1976, Section 12.3.1.
38. I. J. Chen, G. E. Hagler, L. E. Abbott, D. C. Bogue, and J. L. White, ‘‘Interpretation of Tensile and Melt Spinning Experiments in LDPE and HDPE,’’ Trans. Soc. Rheol., 16, 473 (1972).
39. J. L White and Y. Ide, ‘‘Instabilities and Failure in Elongational Flow and Melt Spinning of Fibers,’’ J. Appl. Polym. Sci. 22, 3057–3074 (1978).
40. B. M. Kim, J. C. Hyun, J. S. Oh, and S. J. Lee, ‘‘Kinematic Waves in the Isothermal Melt Spinning of Newtonian Fluids,’’ AIChE J., 42, 3134–3169 (1996).
41. H. W. Jung, H.-S. Song, and J. C. Hyun, ‘‘Draw Resonance and Kinematics Waves in Viscoelastic Isothermal Spinning,’’ AIChE J., 46, 2106–2111 (2000).
42. J. R. A. Pearson and C. J. S Petrie, ‘‘The Flow of a Tubular Film. Part 1. Formal Mathematical Presentation,’’ J. Fluid Mech., 40, 1–19 (1970).
43. J. R. A. Pearson and C. J. S Petrie, ‘‘The Flow of a Tubular Film. Part 2. Interpretation of the Model and Discussion of Solutions,’’ J. Fluid Mech., 42, 609–625 (1970).
44. J. R. A. Pearson and C. J. S. Petrie, Plast. Polym., 38, 85 (April 1970).
45. C. J. S. Petrie, ‘‘A Comparison of Theoretical Predications with Published Experimental Measurements on the Blown Film Process,’’ AIChE J., 21, 275–282 (1975).
46. W. Ast, ‘‘Der Abka¨lvorgang bein Herstellen von Blasfolien aus Polya¨thylen Niedriger Dichte,’’ Kunststoffe, 63, 427 (1973).
47. C. J. S. Petrie, in Computational Analysis of Polymer processing, J. R. A Pearson and S. M. Richardson, Eds., Applied Science Publishers, New York, 1983, Chapter 7.
48. J. R. A. Pearson, Mechanics of Polymer Processing, Applied Science Publishers, New York, 1985.
49. C. D. Han and J. Y. Park, ‘‘Studies on Blown Film Extrusion, I. Experimental Determination of Elongational Viscosity,’’ J. Appl. Polym. Sci., 19, 3257 (1975).
50. C. D. Han and J. Y. Park, ‘‘Studies on Blown Film Extrusion, II. Analysis of the Deformation and Heat Transfer Process,’’ J. Appl. Polym. Sci., 19, 3277 (1975).
51. C. D. Han and J. Y. Park, ‘‘Studies on Blown Film Extrusion, III. Bubble Instability. Analysis of the Deformation and Heat Transfer Process,’’ J. Appl. Polym. Sci., 19, 3291 (1975).
52. R. K. Gupta, Ph.D. Thesis, Department of Chemical Engineering, University of Delaware, Newark, NJ 1980.
53. T. Kanai and J. L. White, ‘‘Kinematics, Dynamics and Stability of the Tubular Film Extrusion of Various Polyethylenes,’’ Polym. Eng. Sci., 24, 1185–1201 (1984).
54. T. Kanai and J. L. White, ‘‘Dynamics, Heat Transfer, and Structure Development in Tubular Film Extrusion of Polymer Melts: A Mathematical Model and Prediction,’’ J. Polym. Eng., 5, 135 (1985).
55. V. Sidiropoulos and J. Vlachopoulos, ‘‘An Investigation of Venturi and Coanda Effects in Blown Film Cooling,’’ Int. Polym. Process., 15, 40 (2000).
56. V. Sidiropoulos and J. Vlachopoulos, ‘‘The Effect of Dual-orifice Air-ring Design on Blown Film Cooling,’’ Polym. Eng. Sci., 40, 1611–1618 (2000).
57. V. Sidiropoulos and J. Vlachopoulos, ‘‘Numerical Study of Internal Bubble Cooling in Film Blowing,’’ Int. Polym. Process., 16, 48–53, (2001).
58. V. Sidiropoulos and J. Vlachopoulos, ‘‘Temperature Gradients in Blown Film Bubbles,’’ Adv. Polym. Technol., 24, 83–90 (2005).
59. G. A. Campbell, N. T. Obot, and B. Cao ‘‘Aerodynamics in the Blown Film Process,’’ Polym. Eng. Sci., 32, 751 (1992).
60. X.-L. Luo and R. I. Tanner, ‘‘A Computer Study of Film Blowing,’’ Polym. Eng. Sci., 25, 620–629 (1985).

61. A. I. Leonov, ‘‘Nonequilibrium Thermodynamics and rheology of viscoelastic polymer media,’’ Rheol. Acta, 15, 85–98 (1976).
62. J. J. Cain and M. M. Denn, ‘‘Multiplicity and Instabilities in Film Blowing,’’ Polym. Eng. Sci., 28, 1527–1541 (1988).
63. D. Acierno, F. P. La Mantia, G. Marrucci, and G. Titomanlio, ‘‘A Non-linear Viscoelastic Model with Structure-dependent Relaxation Times: I. Basic Formulation, ’’ J. Non-Newt. Fluid Mech., 1, 125–146 (1976).
64. C. D. Han, Rheology in Polymer Processing, Academic Press, New York, 1976, fig. 9.14.
65. J. C. Hyun, H. Kim, J. C. Lee, H. S. Song, and H. W. Jung, ‘‘Transient Solutions of the Dynamics in Film Blowing Processes,’’ J. Non-Newt. Fluid Mech., 121, 157–162 (2004).
66. G. N. Beall and J. L. Throne, Hollow Plastics Parts: Manufacturing and Design, Hanser, New York, 2004.
67. D. V. Rosato, A. V. Rosato, and D. P. DiMatia, Blow Molding Handbook, Second Edition, Hanser, Munich, 2003.
68. M. L. Druin, ‘‘PET Properties and Performance Requirements,’’ paper presented at the Polyester Packaging - The Critical Path Ahead Conference, sponsored by Packaging Strategies, Inc., Newark, NJ, May 28–30 (1997).
69. N. Sheptak and C. E. Beyer, ‘‘Study of Parison Formation, including the Effects of Swell and Drawdown,’’ Soc. Plastics Eng. J., 32, 190–196 (1965).
70. M. R. Kamal, V. Tan, and D. Kalyon, ‘‘Measurement and Calculation of Parison Dimensions and Bottle Thickness Distribution during Blow Molding,’’ Polym. Eng. Sci., 21, 331–338 (1981).
71. M. R. Kamal and D. M. Kalyon, ‘‘An Experimental Investigation of Capillary Extrudate Swell in Relation to Parison Swell Behavior in Blow Molding,’’ Polym. Eng. Sci., 26, 508–516 (1986).
72. A. Gracia-Rejon, R. W. DiRaddo, and M. E. Ryan, ‘‘Effect of Die Geometry and Flow Characteristics on Viscoelastic Annular Die Swell,’’ J. Non-Newt. Fluid Mech., 60,107–128 (1995).
73. N. Orbey and J. M. Dealy, ‘‘Isothermal Swell of Extrudate from Annular Dies; Effects of Die Geometry, Flow Rate, and Resin Characteristics,’’ Polym. Eng. Sci., 24, 511–518 (1984).
74. J. M. Dealy and N. Orbey, ‘‘A Model for Parison Behavior in the Extrusion Blow Molding Process,’’ AIChE J., 31, 807–811 (1985).
75. A. H. Wagner and D. Kalyon, ‘‘Parison Formation and Inflation Behavior of Polyamide-6 during Extrusion Blow Molding,’’ AIChE J., 36, 1897–1906 (1996).
76. D. Laroche, K. K. Kabanemi, L. Pecora, and R.W. DiRaddo, ‘‘Integrated Numerical Modeling of the Blow Molding Process,’’ Polym. Eng. Sci., 39, 1223–1233 (1999).
77. S. Tanue, T. Kajiwara, K. Funatsu, K. Terada, and M. Yamabe, ‘‘Numerical Simulation of Blow Molding – Prediction of Parison Diameter and Thickness Distribution in the Parison Formation Process,’’ Polym. Eng. Sci., 36, 2008–2017 (1996).
78. Y. Otsuki, T. Kajiwara, and K. Funatsu, ‘‘Numerical Simulations of Annular Extrudate Swell Using Various Types of Viscoelastic Models,’’ Polym. Eng. Sci., 39, 1969–1981 (1999).
79. B. Bernstein, E. A. Kearsley, and L. J. Zappas, ‘‘A Study of Stress Relaxation with Finite Strain’’, Trans. Soc. Rheol. 7, 391–410 (1963).
80. M. H. Wagner, T. Raible, and J. Meissner, ‘‘Tensile Overshoot in Uniaxial Extension of LDPE Melt,’’ Rheol. Acta, 18, 427–428 (1979).
81. J. T. Oden and T. Sato, ‘‘Finite Strains and Displacements of Elastic Membranes by the Finite Element Method,’’ Int. J. Solids and Struct., 3, 471–488 (1967).
82. J. M. A. Cesar de Sa, ‘‘Numerical Modeling of Glass Forming Processes,’’ Eng. Comput., 3, 266-275 (1986).
83. C. D. Denson, ‘‘Implications of Extentioal Flow in Polymer Fabrication Processes,’’ Polym. Eng. Sci., 13, 125 (1973).
84. C. J. S. Petrie and K. Ito, ‘‘Prediction of Wall Thickness of Blow Molded Containers,’’ Plast. Rubber Process., 5, 68-72 (1980).
85. H. G. deLorenzi and H. F. Nied, ‘‘Finite Element Simulation of Thermoforming and Blow Molding,’’ SPE ANTEC Tech. Papers, 33, 418–420 (1987).
86. H. G. deLorenzi and H. F Nied, ‘‘Blow Molding and Thermoforming of Plastics: Finite Element Modeling,’’ Compu. Struct. 26, 197–206 (1987).
87. H. G. deLorenzi, H. Nied, and C. A. Taylor, ‘‘Simulation and Analysis of Blow Molding Using the Finite Element Method,’’ SPE ANTEC Tech. Papers, 34, 797–799 (1988).
88. H. F. Nied, C. A. Taylor, and H. G. deLorenzi, ‘‘Three-dimensional Finite Element Simulation of Thermoforming,’’ Polym. Eng. Sci., 30, 1314–1322 (1990).
89. H. G. deLorenzi and H. F Nied in Progress in Polymer Processing, A. I. Isayev, Ed., Hanser Verlag, Munich, 1991.
90. J. M. Charrier, S. Shrivastava, and R. Wu, ‘‘Free and Constrained Inflation of Elastic Membranes in Relation to Thermoforming - non-axisymmetric Problems,’’ J. Strain Anal., 24, 55–74 (1989).
91. G. Marckmann, E. Verron, and B. Peseux, ‘‘Finite Element Analysis of Blow Molding and Thermoforming Using a Dynamic Explicit Procedure,’’ Polym. Eng. Sci., 41, 426–439 (2001).

92. E. Verron, G. Marckmann, and B. Peseux, ‘‘Dynamic Inflation of Non-Linear Elastic and Viscoelastic Rubber-like Membranes,’’ Int. J. Num. Meth. Eng. 50, 1233–1251 (2001).
93. D. Laroche, K. K. Kabanemi, L. Pecora, and R. W. Diraddo, ‘‘Integrated Numerical Modeling of the Blow Molding Process,’’ Polym. Eng. Sci., 39, 1223–1233 (1999).
94. M. H. Vantal, B. Monasse, and M. Bellet, Numiform, 95, 1089 (1995).
95. A. Rodriguez-Villa, J. F. Agassant, and M. Bellet, ‘‘Finite Element Simulation of the Extrusion Blow-Molding Process,’’ Numiform, 95, 1053 (1995).
96. S. Wang , A. Makinouchi, and T. Nakagawa, ‘‘Three-dimensional Viscoplastic FEM Simulation of a Stretch Blow Molding Process,’’ Adv. Polym. Technol., 17, 189–202 (1998).
97. K. Kouba and J. Valchopoulos, ‘‘Modeling of Thermoforming and Blow Molding,’’ Theoretical and Applied Rheology, Proc. XIth Cong. Rheology, Brussels, Belgium, August 17–21, 1992.
98. B. Debbaut, B. Hocq, and J. M. Marchal, ‘‘Numerical Simulation of the Blow Molding Process,’’ SPE ANTEC Tech. Papers, 39, 1870–1872 (1993).
99. B. Debbaut, B. Hocq, J. M. Marchal, Y. Jiang, and V. Legat, ‘‘Blow Molding: a 3D Approach,’’ Proc. IIIWorld Congr. on Computational Mechanics, IACM, Chiba, Japan, 1994, pp. 1580–1581.
100. S. Shrivastava and J. Tang, ‘‘Large Deformation Finite Element Analysis of Non-linear Viscoelastic Membranes With Reference to Thermoforming,’’ J. Strain Anal. 28, 31 (1993).
101. D. Laroche, K. K. Kabanemi, L. Pecora, and R.W. DiRaddo, ‘‘Integrated Numerical Modeling of the Blow Molding Process,’’ Polym. Eng. Sci., 39, 1223–1233 (1999).
102. F. M. Schmidt, J. F. Aggasant, and M. Bellet, ‘‘Experimental Study and Numerical Simulation of the Injection Stretch/Blow Molding Process,’’ Polym. Eng, Sci., 38, 1399–1407 (1998).
103. M. F. Edwards, P. K Suvanaphen, and W. L. Wilkinson, ‘‘Heat Transfer in Blow Molding Operations,’’ Polym. Eng. Sci. 19, 910 (1979).

104. M. F. Edwards, S. Georghiades, and P. K. Suvanaphen, Plast. Rubber. Compos. Process. Appl., 1, 161 (1981).
105. M. R. Kamal and D. Kalyon, ‘‘Heat Transfer and Microstructure in Extrusion Blowmolding,’’ Polym. Eng. Sci., 23, 503–509 (1983).